*Exploration Geophysics (2004) **35**, 51–55*
Butsuri-Tansa (Vol. 57, No. 1)
Mulli-Tamsa (Vol. 7, No. 1)

Efficient crosswell EM Tomography using localized nonlinear approximation

Hee Joon Kim[1] Yoonho Song[2] Ki Ha Lee[3] Michael J. Wilt[4]

Key Words: crosswell, LN approximation, electromagnetic, cylindrical symmetry, inversion

ABSTRACT

This paper presents a fast and stable imaging scheme using the localized nonlinear (LN) approximation of integral equation (IE) solutions for inverting electromagnetic data obtained in a crosswell survey. The medium is assumed to be cylindrically symmetric about a source borehole, and to maintain the symmetry a vertical magnetic dipole is used as a source. To find an optimum balance between data fitting and smoothness constraint, we introduce an automatic selection scheme for a Lagrange multiplier, which is sought at each iteration with a least misfit criterion. In this selection scheme, the IE algorithm is quite attractive for saving computing time because Green's functions, whose calculation is a most time-consuming part in IE methods, are repeatedly re-usable throughout the inversion process. The inversion scheme using the LN approximation has been tested to show its stability and efficiency, using both synthetic and field data. The inverted image derived from the field data, collected in a pilot experiment of water-flood monitoring in an oil field, is successfully compared with that derived by a 2.5-dimensional inversion scheme.

INTRODUCTION

High-resolution imaging of electrical conductivity has been the subject of many studies in crosswell tomography using electromagnetic (EM) fields (Zhou et al., 1993; Wilt et al., 1995; Alumbaugh and Morrison, 1995; Newman, 1995; Alumbaugh and Newman, 1997). Although the theoretical understanding of, and associated field practices for, crosswell EM methods are relatively mature, fast and stable inversion of crosswell EM data is still a challenging problem.

Since Raiche (1974) first formulated a three-dimensional (3D) volume integral equation (IE) method, many numerical solutions have been presented on this subject (Hohmann, 1988). The main advantage of the IE method over the finite difference (FD) and finite-element (FE) methods is its greater suitability for inversion. For example, the IE formulation includes a sensitivity matrix, which can be revised at each inversion iteration at little cost. With the FD or FE method, in contrast, the sensitivity matrix must be recomputed at each iteration at a cost nearly equal to that of full forward modelling. The IE method, however, must overcome a severe practical limitation imposed on the size of the imaging domain for inversion purposes. To do this, several approximate methods such as the localized nonlinear (LN) approximation (Habashy et al., 1993) and the quasi-linear approximation (Zhdanov and Fang, 1996) have been developed. Recently, Lee et al. (2002) applied the LN approximation for a cylindrically symmetric model to inverting single-hole EM data.

In this paper an advantage of the LN approximation of the cylindrically symmetric IE solution is further exploited, with application to crosswell EM tomography. We begin our discussion with a critical check of the accuracy of the LN approximation for a cylindrically symmetric model. We then describe our EM inversion algorithm and demonstrate its stability and effectiveness by inverting synthetic data. Finally, we present an example application to field data obtained as a part of a pilot project of water-flood monitoring at the Lost Hills oil field in central California, U.S.A.

THE LN APPROXIMATION

The LN approximation of IE solutions for a cylindrically symmetric model is described in detail in Lee et al. (2002). For completeness, the algorithm is briefly outlined here.

Assuming an $e^{+i\omega t}$ time dependency and neglecting displacement currents, an IE solution for the electric field $\mathbf{E}(\mathbf{r})$ at $\mathbf{r}$ can be written as

$$\mathbf{E}(\mathbf{r}) = \mathbf{E}_b(\mathbf{r}) - i\omega\mu \int_V \mathbf{G}_E(\mathbf{r}-\mathbf{r}') \cdot \Delta\sigma(\mathbf{r}')\mathbf{E}(\mathbf{r}')dv' , \qquad (1)$$

where $\mathbf{E}_b(\mathbf{r})$ is the background electric field, $\mathbf{G}_E(\mathbf{r}-\mathbf{r}')$ the electric Green's tensor, σ the electrical conductivity, ω the angular frequency, and μ the magnetic permeability (Hohmann, 1975). In equation (1), $\Delta\sigma(\mathbf{r}')$ inside the integral represents the excess conductivity, $\sigma(\mathbf{r}')-\sigma_b$, and the term $\Delta\sigma\mathbf{E}$ is called the scattering current (Hohmann, 1975). Each vector component of the Green's tensor $\mathbf{G}_E(\mathbf{r}-\mathbf{r}')$ is the vector electric field at $\mathbf{r}$ due to a point source at $\mathbf{r}'$ with its current density of $(-i\omega\mu)^{-1}$ A/m^2, polarized in the x, y, and z directions, respectively. To obtain a numerical solution of equation (1), the anomalous body is first divided into a number of cubic cells, and a constant electric field is assigned to each cell (Hohmann, 1988). The process involved in volume IE methods requires computing time proportional to the cube of the number of cells used, and it quickly becomes impractical as the size of the inhomogeneity is increased to handle realistic problems.

The complexity associated with a full 3D problem can be greatly reduced for a model whose conductivity is cylindrically symmetric near a borehole. In order to preserve the cylindrical symmetry in the resultant EM fields, a horizontal loop current source, or a vertical magnetic dipole, may be considered in the borehole. When the problem is formulated using an azimuthal electric field E_φ, which is scalar, the resultant IE solution is

[1] *Department of Environmental Exploration Engineering, Pukyong National University, Busan 608-737, Korea*
Email: hejkim@pknu.ac.kr

[2] *Korea Institute of Geoscience & Mineral Resources, Daejeon 305-350, Korea*

[3] *Ernest Orlando Lawrence Berkeley National Laboratory, Berkeley, CA 94720, U.S.A.*

[4] *ElectroMagnetic Instruments, Inc., Richmond, CA 94804, U.S.A.*

Manuscript received 25 July, 2003.
Revised manuscript received 30 September, 2003.

$$E_\varphi(\mathbf{r}) = E_{\varphi b}(\mathbf{r}) - 2\pi i\omega\mu \iint_{\rho z} G_E(\mathbf{r}-\mathbf{r}')\Delta\sigma(\mathbf{r}')E_\varphi(\mathbf{r}')\rho' d\rho' dz' , \quad (2)$$

where $\mathbf{r} = \vec{\rho} + \vec{z}$ and $\mathbf{r}' = \vec{\rho}' + \vec{z}'$ are the position vectors. The Green's function, which is also scalar, is given in the form of a Hankel transform as

$$G_E(\rho,\rho';z-z') = -\frac{1}{4\pi}\int_0^\infty \frac{e^{-u_b|z-z'|}}{u_b}\lambda J_1(\lambda\rho)J_1(\lambda\rho')d\lambda , \quad (3)$$

where $u_b = (\lambda^2 + i\omega\mu\sigma_b)^{1/2}$ is the vertical wave number and J_1 is the Bessel function of order 1 (Ward and Hohmann, 1988, p. 219). Since measurements are usually made for vertical magnetic fields, equation (2) is modified as

$$H_z(\mathbf{r}) = H_{zb}(\mathbf{r}) - 2\pi i\omega\mu \iint_{\rho z} G_H(\mathbf{r}-\mathbf{r}')\Delta\sigma(\mathbf{r}')E_\varphi(\mathbf{r}')\rho' d\rho' dz' , \quad (4)$$

where $G_H(\mathbf{r}-\mathbf{r}')$ is the magnetic Green's function, which translates the scattering current $\Delta\sigma(\mathbf{r}')E_\varphi(\mathbf{r}')$ at $\mathbf{r}'$ to the magnetic field at $\mathbf{r}$. The magnetic Green's function can be deduced from the corresponding electric Green's function in equation (3) as

$$G_H(\rho,\rho';z-z') = \frac{1}{4\pi i\omega\mu}\int_0^\infty \frac{e^{-u_b|z-z'|}}{u_b}\lambda^2 J_0(\lambda\rho)J_1(\lambda\rho')d\lambda . \quad (5)$$

Using equations (2) through (5), we can obtain an IE solution by first dividing the (ρ, z) cross-section into a number of cells, and then formulating a system of equations for the electric field using a pulse basis function.

The LN approximation offers an efficient and reasonably accurate electric-field solution (Habashy et al., 1993). For the problem where there is only an azimuthal electric field, a good approximation to equation (2) is given by

$$E_\varphi(\mathbf{r}) \approx \gamma(\mathbf{r})E_{\varphi b}(\mathbf{r}) , \quad (6)$$

where

$$\gamma(\mathbf{r}) = \left[1 + 2\pi i\omega\mu \iint_{\rho z} G_E(\mathbf{r}-\mathbf{r}')\Delta\sigma(\mathbf{r}')\rho' d\rho' dz'\right]^{-1} \quad (6a)$$

(Lee et al., 2002).

Substituting equation (6) into equation (4) yields an approximate magnetic-field solution

$$H_z(\mathbf{r}) \approx H_{zb}(\mathbf{r}) - 2\pi i\omega\mu \iint_{\rho z} G_H(\mathbf{r}-\mathbf{r}')\Delta\sigma(\mathbf{r}')\gamma(\mathbf{r}')E_{\varphi b}(\mathbf{r}')\rho' d\rho' dz' . \quad (7)$$

Upon dividing the inhomogeneity into K elements, the secondary magnetic field at the i^{th} receiver may be written as

$$H_{zi}^s \approx -2\pi i\omega\mu \sum_{k=1}^{K} \Delta\sigma_k\gamma_k E_{\varphi bk} \iint_{S_k} G_H(\rho_i,\rho';z_i-z')\rho' d\rho' dz' , \quad (8)$$

where subscript k denotes the k^{th} element and S_k represents the area of the k^{th} element.

To demonstrate the efficiency and usefulness of LN solutions in a crosswell application, let us consider a simple model consisting of a conductive ring about a source borehole in a uniform whole space of 100 Ω.m. The cross-section of the ring is a 10 m x 10 m rectangle and the inner surface is 15 m from the borehole, as shown in Figure 1. Born- and LN-approximated magnetic fields at the other borehole, 50 m from the source borehole, are compared with results obtained from a FE method (Lee et al., 2004).

Figure 2 shows the comparison in secondary vertical magnetic fields between the Born, LN, and FE solutions. The centre of the body is at $z = 0$. The conductivity contrast and operating frequency used are 10 and 10 kHz, respectively. The source and receiver are located at the same depth in each borehole. Greater anomalies can be observed in the imaginary part than in the real part and the LN and FE solutions agree very well.

We are also interested in the quality of LN solutions when the conductivity of the body varies. Figure 3 shows the comparison in secondary vertical magnetic fields between Born, LN, and FE solutions. A vertical magnetic dipole source is fixed at the depth of the centre of the body in the source borehole, and vertical magnetic fields are measured at 10 m below the centre of the body in the receiver borehole. The frequency used is 10 kHz. The LN approximation works very well up to a conductivity contrast of about 100. The imaginary part of the LN solution starts deviating from the FE solution beyond a conductivity contrast of 100, while the real part still shows a good agreement.

Finally, a comparison of responses as frequency is varied is shown in Figure 4. The source–receiver array is the same as that in Figure 3 and the conductivity contrast is fixed at 10. The LN and FE solutions show a good agreement all the way up to about 100 kHz. From these forward solutions we can conclude that the LN approximation has sufficient accuracy for a practical application.

CROSSWELL TOMOGRAPHY

Based on the encouraging results on the LN approximation as described above, we have proceeded to implement a crosswell EM inversion scheme. For the inversion, the sensitivity of the magnetic field with respect to the change in conductivity can be easily obtained from equation (8). Taking the derivative of the magnetic field with respect to the j^{th} conductivity parameter, and neglecting the dependence of γ_j on $\Delta\sigma_j$, the sensitivity becomes

$$\frac{\partial H_{zi}^s}{\partial\sigma_j} \approx -2\pi i\omega\mu\gamma_j E_{\varphi bj} \iint_{S_j} G_H(\rho_i,\rho';z_i-z')\rho' d\rho' dz' , \quad (9)$$

which can be easily evaluated by integrating the magnetic Green's function over the area of the j^{th} cell.

The inversion procedure starts with the data misfit $\|\mathbf{W}_d[\mathbf{H}(\sigma) - \mathbf{H}_d]\|^2$, where $\|\bullet\|^2$ denotes the L_2 norm, $\mathbf{W}_d$ is the data weighting matrix and subscript d denotes data. If the conductivity is perturbed by $\delta\sigma$, the misfit becomes $\|\mathbf{W}_d[\mathbf{H}(\sigma + \delta\sigma) - \mathbf{H}_d]\|^2$, and a total objective function can be written as

$$\phi = \left\|\mathbf{W}_d[\mathbf{H}(\sigma+\delta\sigma) - \mathbf{H}_d]\right\|^2 + \lambda\left\|\mathbf{W}_\sigma\delta\sigma\right\|^2 . \quad (10)$$

Here the second term on the right-hand side is added to impose a smoothness constraint, $\mathbf{W}_\sigma$ is the weighting matrix for σ, and λ is the Lagrange multiplier that controls the trade-off between data misfit and parameter smoothness. Expanding the misfit in $\delta\sigma$ using the Taylor series, discarding terms higher than the second-order term, and letting the derivative of the function with respect to $\delta\sigma$ equal zero, we obtain a linear system of normal equations for the perturbation $\delta\sigma$:

$$(\mathbf{J}^T\mathbf{W}_d^T\mathbf{W}_d\mathbf{J} + \lambda\mathbf{W}_\sigma^T\mathbf{W}_\sigma)\delta\sigma = -\mathbf{J}^T\mathbf{W}_d^T\mathbf{W}_d[\mathbf{H}(\sigma) - \mathbf{H}_d] , \quad (11)$$

where superscript T indicates the matrix transpose, and the entries of Jacobian matrix $\mathbf{J}$ are the sensitivity functions given in equation (9).

Inversion stability is largely controlled by requiring the conductivity to vary smoothly. Larger values of λ result in smooth and stable solutions at the expense of resolution. Such values even allow for the solution of grossly underdetermined problems (Tikhonov and Arsenin, 1977). In this crosswell tomography, we employ the Occam approach, first proposed by Constable et al. (1987), to determine an optimum λ during the inversion process

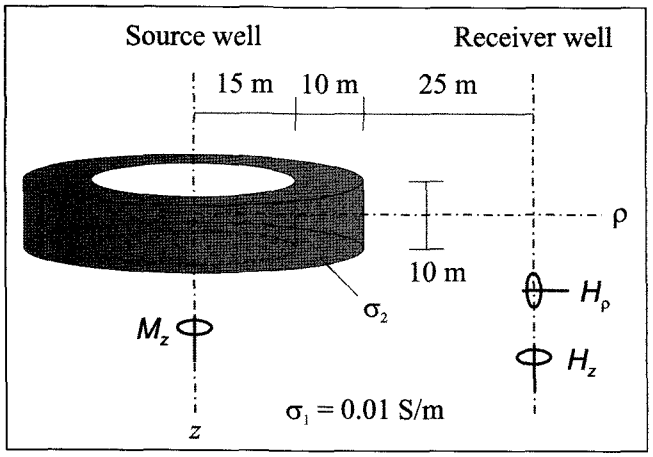

Fig. 1. A cylindrically symmetric model. A conductive body with a cross-section of 10 m x 10 m is cylindrically symmetric about a vertical source borehole, with the inner surface 15 m away from the borehole, in a whole space of 0.01 S/m. Magnetic fields from a vertical magnetic dipole source in that borehole are measured in the other borehole, 50 m horizontally away from the source borehole.

(see also deGroot-Hedlin and Constable, 1990; Parker, 1994). The unique feature of the Occam approach is that the parameter λ is used at each iteration both as a step length control and as a smoothing parameter. That is, equation (11) is solved for a series of trial values of λ and the root-mean-square (rms) misfit for each λ is evaluated by solving the 2D forward problem. The Occam process then chooses the model with minimum misfit as the basis for the next iteration. The minimisation can be carried out by means of a simple 1D line search. In this selection scheme, IE modelling is quite attractive in speed because Green's functions for the electric field involving the Hankel transform, the most time-consuming part in IE methods, are repeatedly re-usable throughout the selection procedure. In this study, the selection of an optimum λ is based on three trial values, and therefore three forward models, at each iteration.

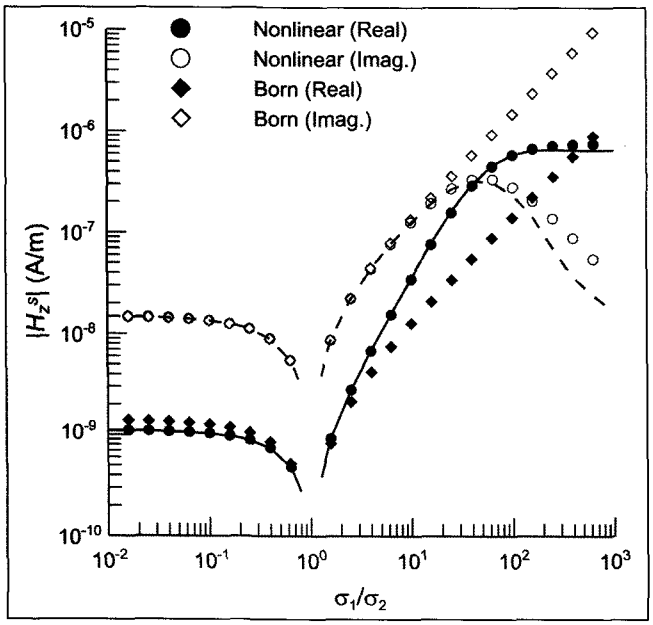

Fig. 3. The effect of conductivity contrast between the body and background on the vertical components of secondary magnetic fields. The depths of source and receiver are fixed at 5 m above and below the bottom of the body, respectively. The operating frequency is 10 kHz. The solid and dashed lines show FE solutions.

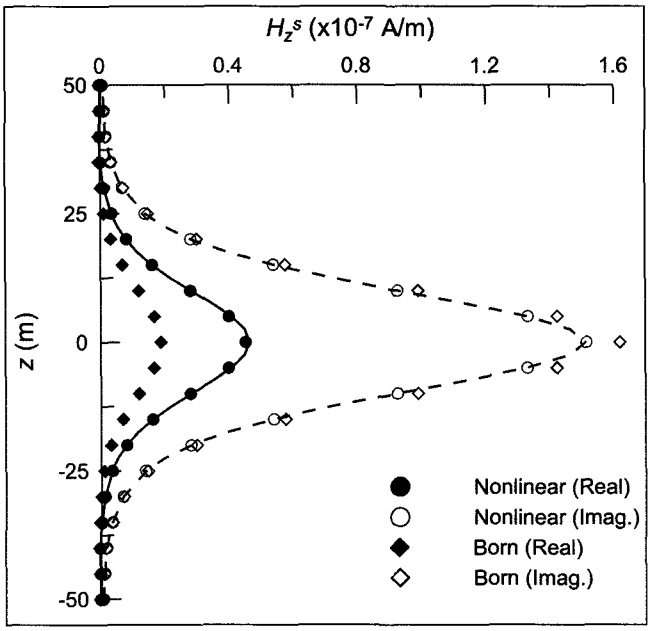

Fig. 2. Vertical components of secondary magnetic fields. The operating frequency is 10 kHz and the conductivity of the body is 0.1 S/m. The array used is a crosswell source–receiver pair keeping the same depth in each borehole. The solid and dashed lines show FE solutions.

To evaluate the performance of crosswell tomography using the LN approximation, we choose the conductivity model shown in Figure 5. The model consists of two cylindrically symmetric bodies, one conductive (0.1 S/m), and the other resistive (0.001 S/m), in a whole space of 0.01 S/m. A FE scheme (Lee et al., 2004) is used to generate synthetic data. Using a vertical magnetic dipole (M_z) as a source, vertical magnetic fields (H_z) are computed at three frequencies: 2.5 kHz, 10 kHz, and 20 kHz. Three-percent Gaussian noise is added to the synthetic data prior to the inversion. The inversion is started with an initial model of uniform 60 Ω.m resistivity throughout the whole space.

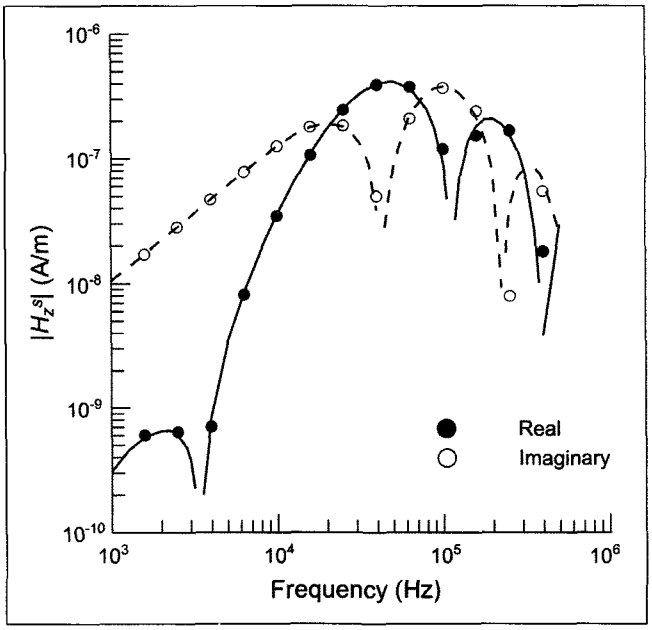

Fig. 4. The effect of frequency on the vertical components of secondary magnetic fields. The depths of source and receiver are fixed at 5 m above and below the bottom of the body, respectively. The conductivity of the body is 0.1 S/m.

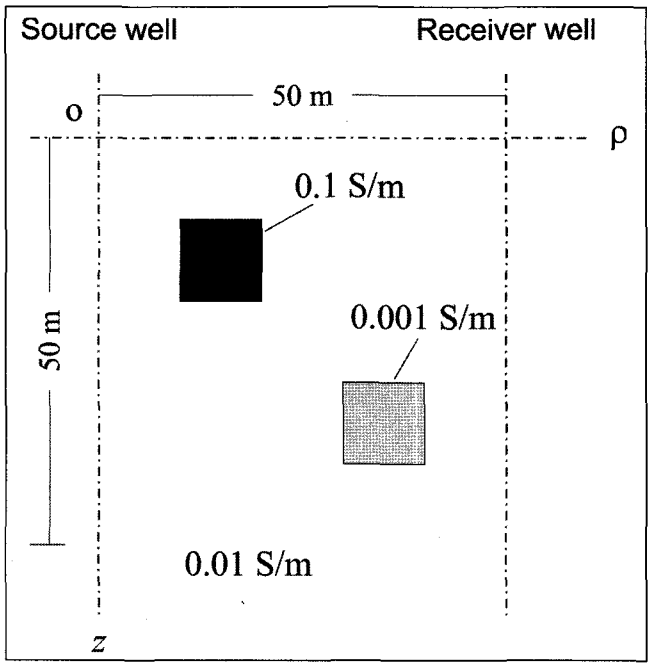

Fig. 5. A model used to calculate synthetic data for inversion test. Two rings of 0.1 S/m and 0.001 S/m, separated vertically by 10 m, are located in a whole-space of 0.01 S/m. The upper and lower bodies are horizontally 10 m and 30 m away from the source borehole, respectively.

as shown in Figure 6. The recovered conductivity in the region of the conductive body is found to be nearly the same as in the original model, but is overestimated in the region of the resistive body. The inversion process is quite stable and the rms misfit decreases from the initial guess of 5.095 to 0.032 after seven iterations (Figure 7). The smoothing parameter varies greatly during the inversion process. This means that it is difficult to determine this parameter a priori.

Finally, our inversion algorithm has been applied to a set of crosswell EM data collected as a part of water-flood monitoring at the Lost Hills oil field in central California (Wilt et al., 2001). Two fibreglass-cased wells were installed at the southern margin of the oil field for the monitoring and the separation between these two observation wells is 82 m. Although EM data before and after injection of water are available, we analyze only the pre-injection EM data. The data were H_z measurements from M_z sources. The operating frequency was 1 kHz.

A 2D inversion result is shown in Figure 8 along with a 2.5D inversion result for comparison. The 2.5D inversion scheme also uses the LN approximation for both forward and sensitivity calculations (Song et al., 2001). For the sake of comparison, we use no geological information to constrain the crosswell data inversion, except for the smoothness constraint. The cell size for these images is 5 m x 5 m. The initial model used is a 1.4 Ω.m uniform whole space, and after five iterations, the rms misfit is reduced to less than 10%. Both methods give similar images in spite of different model dimensions. Alumbaugh and Morrison (1995) showed that the effects of structures outside the interwell plane are minimised for borehole separations greater than five skin depths. As the minimum separation between source and receiver in our case is about 4.5 times greater than the skin depth (about 19 m), reconstructed images are expected to have few artefacts, and the approximation of 2D cylindrical geometry can provide similar results to those other schemes but at much less computational cost. Computing time required for this 2D approximate inversion is less than 5 minutes, to obtain 588

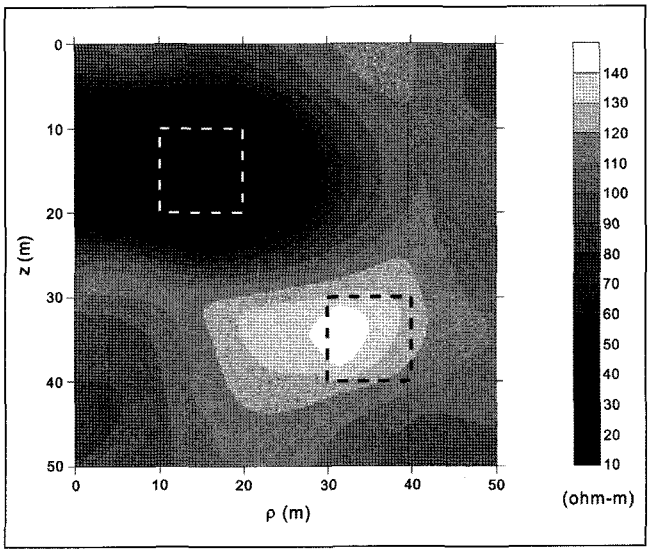

Fig. 6. An image of the two bodies reconstructed from the inversion of synthetic data, after seven iterations.

conductivities from 1368 complex H_z data, on a Pentium IV, 1.5 GHz processor with 512 MB of RAM, compared to about 2 days for the 2.5D inversion.

CONCLUSIONS

The LN approximation of IE solutions has been applied to inverting crosswell EM data, using a cylindrically symmetric model. When the LN approximation is applied to the cylindrically symmetric model with a vertical magnetic dipole source, it works very well because electric fields are scalar and continuous everywhere. One of the most important steps in the inversion is the selection of a proper regularization parameter for stability. The LN solution provides an efficient means for selecting an optimum regularization parameter, because Green's functions, the most time-consuming part in IE methods, are repeatedly re-usable at

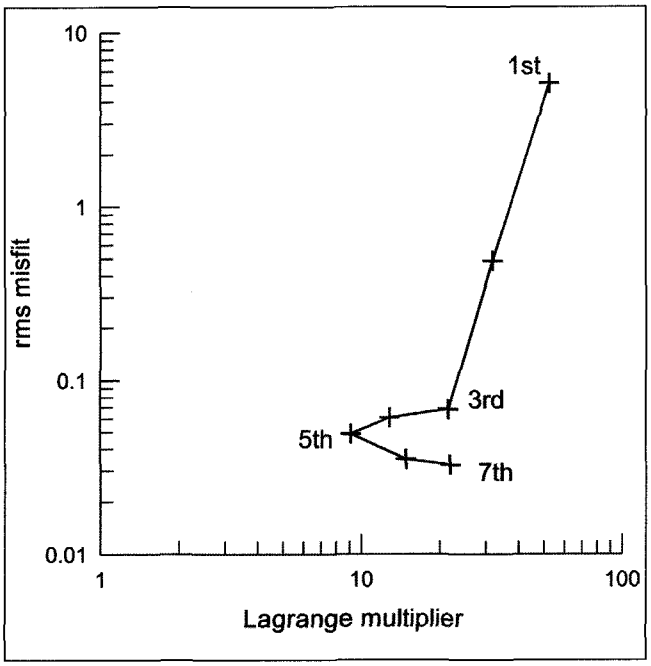

Fig. 7. Convergence in rms misfit, and the associated Lagrange multiplier at each iteration, during the synthetic model inversion.

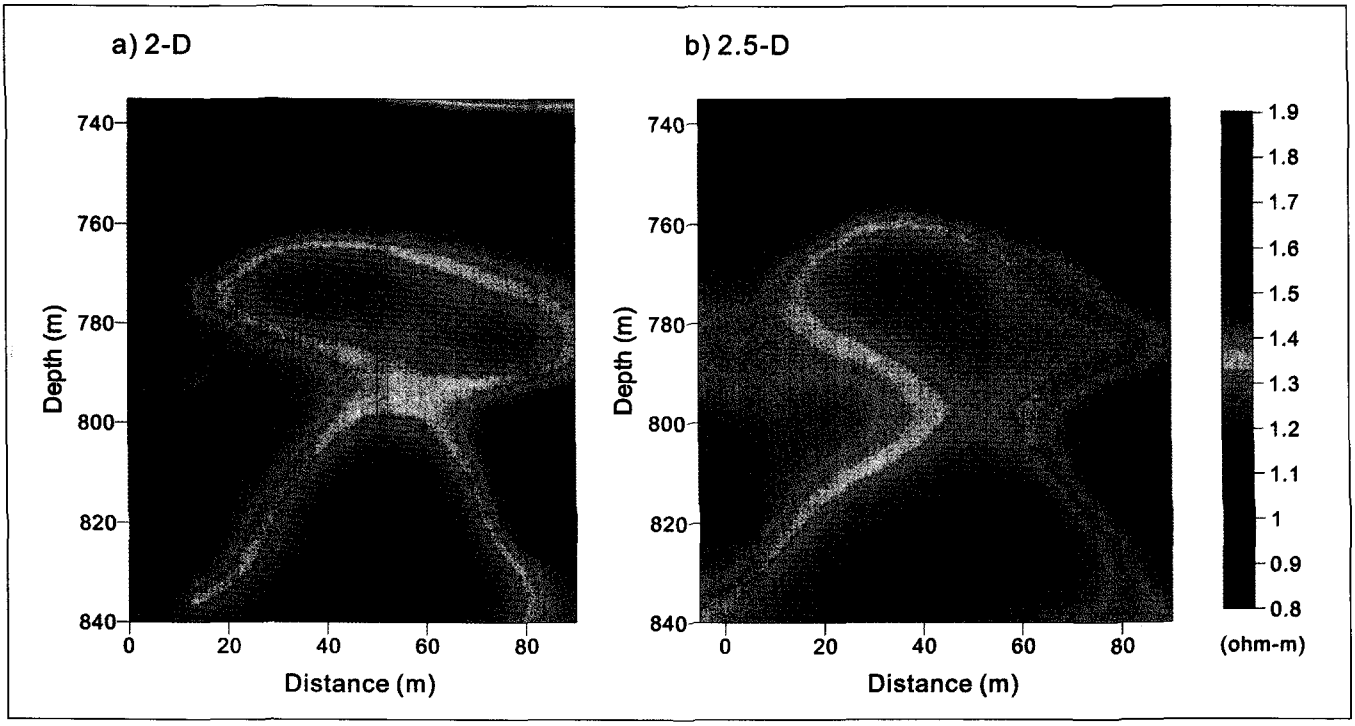

Fig. 8. Comparison of resistivity images derived from the 2D (a) and 2.5D (b) inversion of crosswell EM data collected at the Lost Hills oil field in central California. The pixel size for these images is 5 m x 5 m and the initial model is a homogeneous whole space of 1.4 Ω.m.

each iteration. The stability and efficiency of this fast imaging scheme has been tested using both synthetic and field data. The reconstructed image from the field data, obtained in a pilot study for water-flood monitoring at the Lost Hills oil field, matched well with that of the 2.5D inversion scheme.

ACKNOWLEDGEMENTS

This study was partially supported by a Pukyong National University Research Foundation Grant in 2003. Y. Song's work was supported by the Korean Ministry of Science and Technology through National Research Lab. Funding. K. H. Lee is a collaborator whose work was partially supported by the Assistant Secretary for Energy Efficiency and Renewable Energy, Office of Wind and Geothermal Technologies of the U.S. Department of Energy, under Contract No. DE-AC03-76SF00098.

REFERENCES

Alumbaugh, D.L. and Morrison, H.F., 1995, Theoretical and practical considerations for crosswell electromagnetic tomography assuming a cylindrical geometry: *Geophysics*, **60**, 846–870.

Alumbaugh, D.L., and Newman, G.A., 1997, Three-dimensional massively parallel electromagnetic inversion - II. Analysis of crosswell electromagnetic experiment: *Geophys. J. Int.*, **128**, 355–363.

Constable, S.C., Parker, R.L., and Constable, C.G., 1987, A practical algorithm for generating smooth models from electromagnetic sounding data: *Geophysics*, **52**, 289–300.

deGroot-Hedlin, C., and Constable, S.C., 1990, Occam's inversion to generate smooth, two-dimensional models from magnetotelluric data: *Geophysics*, **55**, 1613–1624.

Habashy, T.M., Groom, R.M., and Spies, B.R., 1993, Beyond the Born and Rytov approximations: a nonlinear approach to electromagnetic scattering: *J. Geophys. Res.*, **98**, 1795–1775.

Hohmann, G.W., 1975, Three-dimensional induced polarization and EM modeling: *Geophysics*, **40**, 309–324.

Hohmann, G.W., 1988, Numerical modeling for electromagnetic methods of geophysics, in Nabighian, M.N., (ed.), *Electromagnetic Methods in Applied Geophysics*, Vol. 1: Soc. Expl. Geophys., 313–363.

Lee, K.H., Kim, H.J., and Uchida, T., 2004, Electromagnetic fields in steel-cased borehole: *Geophys. Prosp.*, **52**, (in press).

Lee, K.H., Kim, H.J., and Wilt, M., 2002, Efficient imaging of single-hole electromagnetic data: *GRC Transactions*, **26**, 399–404.

Newman, G.A., 1995, Crosswell electromagnetic inversion using integral and differential equations: *Geophysics*, **60**, 899–911.

Parker, R.L., 1994, *Geophysical Inverse Theory*: Princeton University Press.

Raiche, A.P., 1974, An integral equation approach to 3D modeling: *Geophys. J. Roy. astr. Soc.*, **36**, 363–376.

Song, Y., Kim, J.-H., and Chung, S.-H., 2001, An efficient 2.5-D inversion of loop-loop EM data, *Proc. 5th SEGJ Int. Symp.*, 153–160.

Tikhonov, A.N., and Arsenin, V.Y., 1977, *Solutions to Ill-Posed Problems*: John Wiley and Sons, Inc.

Ward, S.H., and Hohmann, G.W., 1988, Electromagnetic theory for geophysical applications, in Nabighian, M.N., (ed.), *Electromagnetic Methods in Applied Geophysics, Vol. 1*: Soc. Expl. Geophys., 131–311.

Wilt, M.J., Alumbaugh, D.L., Morrison, H.F., Becker, A., Lee, K.H., and Deszcz-Pan, M., 1995, Crosshole electromagnetic tomography: System design considerations and field results: *Geophysics*, **60**, 871–885.

Wilt, M.J., Zhang, P., Osato, K., and Tsuneyama, F., 2001, Crosswell EM studies at the Ellis Lease, Lost Hills California: *Proc. 5th SEGJ Int. Symp.*, 243–250.

Zhdanov, M.S., and Fang, S., 1996, Quasi-linear approximation in 3-D EM modeling: *Geophysics*, **61**, 646–665.

Zhou, Q., Becker, A., and Morrison, H.F., 1993, Audio-frequency electromagnetic tomography in 2-D: *Geophysics*, **58**, 482–495.